Design of a Solar Thermal Propulsion and Power System for Mini-satellite Lunar Orbit Insertion

Leverone, Fiona; Cervone, Angelo; Pini, Matteo; Gill, Eberhard

DOI
10.1109/AERO47225.2020.9172499

Publication date
2020

Document Version
Final published version

Published in
2020 IEEE Aerospace Conference, AERO 2020

Design of a Solar Thermal Propulsion and Power System for Mini-satellite Lunar Orbit Insertion

Fiona Leverone
Department of Space Systems Engineering
Delft University of Technology
Kluyverweg 1, 2629 HS Delft
F.K.Leverone@tudelft.nl

Angelo Cervone
Department of Space Systems Engineering
Delft University of Technology
Kluyverweg 1, 2629 HS Delft
A.Cervone@tudelft.nl

Matteo Pini
Department of Propulsion and Power
Delft University of Technology
Kluyverweg 1, 2629 HS Delft
M.Pini@tudelft.nl

Eberhard Gill
Department of Space Systems Engineering
Delft University of Technology
Kluyverweg 1, 2629 HS Delft
E.K.A.Gill@tudelft.nl

Abstract*—Small satellites with increased capabilities in terms of power and propulsion are being demanded for future missions. This paper proposes a possible solution which is the design of a novel integrated solar thermal system that co-generates propulsion and power on-board mini satellites. The system consists of a solar thermal propulsion system (STP) coupled with a micro-Organic Rankine Cycle (ORC) system to harness the waste heat from the STP receiver to provide electrical power and mitigate the need for solar panels. STP provides an alternative to conventional propulsion systems for missions requiring velocity changes of between 800 m/s and 2500 m/s. Additional advantages include higher specific impulses than chemical propulsion systems, throttability, re-start capabilities, and faster transfer times than electrical propulsion systems. The faster transfer times are especially useful for missions that travel across high radiation regions such as the Van Allen Belt. This unique configuration shares resources such as the concentrator and receiver to potentially extend the power and propulsion capabilities while adhering to the strict mass and volume constraints of small satellites. However, there is currently no literature available on the design process of the proposed bi-modal system. This paper therefore presents an integrated solar thermal design strategy for a Geostationary Transfer Orbit to Lunar orbit insertion mission. The design methodology is described in detail to assist with future evaluations of integrated solar thermal systems for other applications and missions. The system is designed to provide a velocity increment of 1.6 km/s. Five mini-satellite sizes were investigated with a gross wet mass of 100 kg, 200 kg, 300 kg, 400 kg, and 500 kg respectively. Each satellite requires to produce an electrical power of 1 W/kg. The STP system uses water as the propellant due to its safety and performance attributes. Toluene has been selected as the working fluid for the ORC due to its high thermal efficiency. By incorporating the use of a high-temperature receiver, propellant temperatures around 2500 K can be achieved that can produce high specific impulse values of more than 300 s. The design has been optimized for various design parameters, such as propellant temperature, nozzle area ratio, burn time, concentrator design, and ORC cycle pressures. The optimization provides an initial framework in the selection of an optimal integrated solar thermal design for the proposed Lunar mission. An analysis of variance has also been conducted to identify which system parameters, such as optical efficiency and turbine efficiency, have the most influential effect on the system. The heaviest components of the system are the propellant (40 to 50%), concentrator (8%), and insulation (8%) with respect to the gross mass of the satellite.

TABLE OF CONTENTS

978-1-7281-2734-7/20/$31.00 ©2020 IEEE

1. INTRODUCTION

There is an increasing demand for small satellites to have higher on-board electrical power and propulsion capabilities for future interplanetary missions. NASA has suggested that target power densities and specific energies for electrical power system on-board future interplanetary spacecraft are between 150 and 250 W/kg [1] and more than 250 Wh/kg [2]. Conventional small satellite photovoltaic technologies are around 20 to 100 W/kg [3, 4] and Lithium-polymer and –ion batteries have specific energies between 150 to 250 Wh/kg. These systems are currently below the targeted values and call for alternative systems to be investigated.

A possible system proposed to meet these specific mission requirements is a bi-modal integrated solar thermal system for propulsion and electrical power generation [5–7]. This novel system for small satellites incorporates a solar thermal propulsion (STP) system and a micro-Organic Rankine Cycle (ORC) system. This integration allows sub-systems to share on-board components as shown in Figure 1, by harvesting energy from the STP system to co-generate electrical power, and possibly use the additional waste heat for on-board thermal control. Solar thermal propulsion systems focus solar radiation onto a receiver or the propellant directly using mirrors or lenses to heat the propellant to very high temperatures, generally between 1000 and 2500 K. The vaporized propellant is then expanded through a nozzle to generate thrust.

Previously, bi-modal solar thermal systems using STP have mainly been coupled with thermionic [8–14] or thermophotovoltaic [15] power conversion systems. Thermionic conversion process operates by transferring electrons from a hot emitter through vacuum to a cooler collector to generate electricity. However, [16] and [17] show that these systems are more suitable for larger power levels. Thermophotovoltaic conversion consists of photovoltaic cells that convert infrared

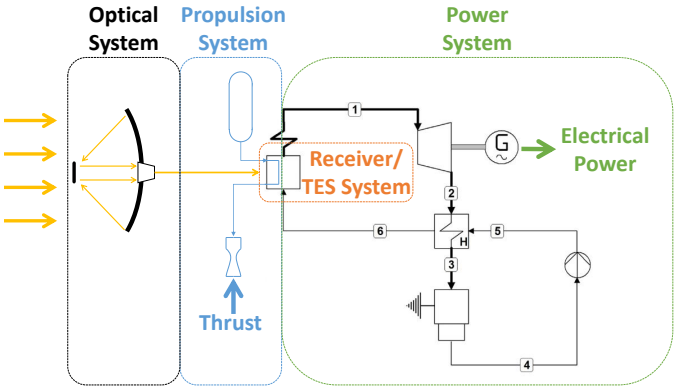

Figure 1. Schematic of the proposed bi-modal solar thermal system.

radiation from a hot thermal emitter into electricity. However, these photovoltaic cells are also vulnerable to degradation in the space environment and therefore not considered.

This research focuses on the use of a micro-ORC system due to its higher resistance to degradation compared to photovoltaic systems [18, 19] and its better thermal efficiency [16] and higher power density compared to micro-Brayton cycles [20]. The lower performance of micro-Brayton cycles is due to the poor compression efficiency as a result to low pressure ratios. Therefore, micro-ORC systems could have smaller and lighter design which is an important criteria for small satellites. ORC power generation systems have been proposed for space applications such as the International Space Station with power capacities ranging from 1 to 30 kW [18, 19]. An ORC is a closed loop cycle that involves an organic working fluid to undergo a phase change and drive a turbine to generate electricity. However, these system do not have flight heritage which increases the risk, and lowers the reliability due to their moving parts compared to static power systems. Additional disadvantages are the fast rotational speeds, supersonic flow in the stator and potential transient inertial effects during start-up and shut-down [21–23]. Thermodynamic processes of the ORC system are illustrated by the numbers indicated in Figure 1. At state 4 the working fluid is a saturated liquid which is then compressed to a higher pressure by the pump to state 5. The regenerator preheats the liquid working fluid to state 6 by using the hot working fluid vapor that exits the turbine (state 2). The receiver vaporizes and superheats the working fluid to state 1.

The influence of design parameters of the proposed integrated solar thermal system are unknown and there is a lack of documented design strategies for this system. Therefore this paper focuses on discussing the design overview of the integrated solar thermal system to provide guidelines for future evaluations. The approach is based on the optimization of the wet system mass as this is a critical parameter for small satellites. Investigation into using an STP and a micro-ORC system for a Geostationary Transfer Orbit (GTO) to Lunar orbit mission for various mini-satellites has been conducted to identify the feasibility and optimal spacecraft mass for this system. The influence of design choices and uncertainty parameters have also been analyzed to increase the reliability of the result due to the lack or limited experimental data available on small-scale flight-weight STP and micro-ORC systems.

2. Mission Selection

Based on previous work [6], it has been found that STP could be useful for future low-cost small satellite missions for high ΔV applications such as a GTO to Lunar orbit transfer mission. This together with the increasing scientific interest in Lunar satellite and habitat missions [24–26], is the main reason for selecting a GTO to Lunar mission for the proposed solar thermal propulsion and power system. The spacecraft is assumed to be launched as a piggyback payload into a supersynchronous geostationary transfer orbit (SSGTO), defined in Table 1, due to the relatively high frequency of more than five per year versus higher orbit launch numbers that occur roughly once per year. This initial orbit also reduces the ΔV required for Earth escape compared to starting at a standard GTO. The purpose of this study is to ensure a fast escape to reduce the exposure of radiation on the spacecraft from the Van Allen belt. Multiple raising maneuvers are investigated to achieve a fast Earth escape while minimizing gravity losses. To minimize the gravity loss, a study on the thrust and burn time combination has been conducted. The system requirements for the bi-modal thermal system are listed in Table 2 with the rationale for each requirement discussed in the following paragraphs.

Table 1. Initial orbital parameters for SSGTO

Initial orbit parameters	Value
Semi-major axis	51 526 km
Eccentricity	0.8705
Inclination	0.01°
Right-ascension of the ascending node	0°
Argument of perigee	0°
True anomaly	0°

The rationale for the STP-01 requirement is based on a conservative ΔV required to complete the following manoeuvres: 1) Earth escape, 2) mid-course correction, 3) Lunar injection burn and 4) orbit maintenance for one year in a low Lunar orbit. Table 3 shows the detailed ΔV budget where values are obtained from literature, an Earth-escape flight trajectory analysis, and includes an additional 10% margin. After Earth escape, a mid-course correction ΔV of 50 to 100 m/s is required to direct the spacecraft to the Moon. To insert a spacecraft into a low near circular lunar orbit of 100 km with an inclination between 30 and 150° a ΔV of approximately 810 to 850 m/s is needed [27–29]. A minimum ΔV of 100 m/s is also required for Lunar maintenance operations due to the lack of certainty of the gravity field for low Lunar orbits with high inclination values [29]. No level of confidence is provided by [27] and [29] for the stochastic maneuvers, the mid-course correction and the Lunar orbit maintenance. A maximum ΔV of 1600 m/s was therefore selected for the mission to increase launch window opportunities.

The thrust is limited to a maximum of 40 N (STP-02) to minimize the disturbance torque and reduce the loading conditions on the inflatable concentrators during orbit transfer. The total thruster burn time is limited to a maximum value of 750 s per burn (STP-03) to reduce the time of exposure of the high-temperature propellant to the nozzle as well as not to limit the disturbance angular momentum. The thrust and time ranges are also restricted to minimize the associated gravity loss to less than 15% as determined during the trajectory analysis. Assuming the maximum allowable thrust vector misalignment, thruster position inaccuracy, and inaccuracy

Table 2. Summary of the key system requirements

ID	Requirement
STP-01	The propulsion system shall provide a minimum ΔV of $1600\,\mathrm{m/s}$.
STP-02	The propulsion system shall have a maximum thrust of $40\,\mathrm{N}$.
STP-03	The propulsion system shall have a maximum thrusting time of $750\,\mathrm{s}$ per orbital manoeuvre.
STP-04	The total time for the Earth escape manoeuvre shall be less than 90 days.
STP-05	The propulsion system shall use nontoxic propellants.
SYS-01	The total wet mass of the integrated system shall be no more than 80% of the spacecraft mass.
POW-01	The electrical power system shall use nontoxic working fluids.
POW-02	The electrical power system shall be able to operate continuously.

Table 3. ΔV Budget

ΔV **Budget**	**Value** [$\mathrm{m\,s^{-1}}$]	**Ref.**
Earth escape	360	Sec. 2
Mid-course correction	50 - 100	[27]
Injection burn	810 - 850	[27–29]
Orbit maintenance (1 yr)	100	[29]
Margin (10%)	132 - 141	
Total	1452 - 1551	

in determining the position of the center of mass are $\pm$1.5 mm, $\pm$1 mm, and $\pm$2.5 mm respectively [30], a worse case total misalignment of 5 mm is assumed. Based on this overall misalignment the disturbance torque is 200 mNm and the angular momentum is 150.2 Nms with the maximum thrust level and burn time. Commercial reaction wheel sets[2] with high torque capability and angular momentum capacity are used to counteract this disturbance along with thrust vectoring for controlling the momentum build-up. The heaviest spacecraft gross mass that will be investigated in this paper is 500 kg, therefore the maximum thrust-to-mass ratio is limited to 0.08.

The maximum total transfer time of 90 days for Earth escape (STP-04) is defined to minimize the radiation exposure to the spacecraft and to compete with the lower range of electric propulsion systems such as the SMART-1 mission that took three months to escape Earth.

Typical combined wet propulsion and electrical power mass fractions for small satellite Delta class planetary missions are between 60 and 75% [31]. Smart-1 was able to achieve a combined wet mass of 54% due to the high specific impulse electric propulsion system on-board. For this study, a slightly higher upper limit, of an additional 5%, is set as the system requirement, SYS-01, due to the low TRL associated with STP and ORC systems for space applications. The low TRL requires higher safety factors and conservative values to be used.

Both the propellant and working fluid selection is limited to nontoxic fluids as the system is assumed to be a secondary payload so reduction in risk is necessary to minimize damage to the primary spacecraft (STP-05 and POW-01). This requirement is further restricted to fluids with a National Fire Protection Association (NPFA) 704 health rating less than 4 [32], such that fluids that can cause fatal injuries are discarded.

[2]RSI 45 Momentum and Reaction Wheels, https://www.rockwellcollins.com/Products-and-Services/Defense/Platforms/Space/RSI-45-Momentum-and-Reaction-Wheels.aspx [Accessed 15 September 2019]

Trajectory analysis

To determine the total time of the Earth escape maneuver, the spacecraft trajectory is calculated by integrating the equations of motion, Equations 1 to 3, assuming a 2-body problem and neglecting perturbations. In this analysis the inputs are the mass of the spacecraft, the vacuum specific impulse, and the initial orbit. During the powered flight of the trajectory the thrust is applied about the perigee with the middle of the burn occurring at perigee. For the coast phase the thrust is set to zero. The equations of motion are

$$\ddot{r} + \frac{\mu}{r^3}\mathbf{r} = \frac{\mathbf{T}}{m} \tag{1}$$

$$\dot{m} = -\frac{|\mathbf{T}|}{I_{sp} g_0} \tag{2}$$

$$\mathbf{T} = u T_{max} \frac{\mathbf{v}}{||\mathbf{v}||} \tag{3}$$

where r is the distance of the satellite from the Earth, μ is the gravitational coefficient of the Earth, m is the mass of the satellite, $\dot{m}$ is the mass flow rate of the propellant, and I_{sp} is the specific impulse. $\mathbf{T}$, T_{max}, u, and $\mathbf{v}$ are the thrust vector, maximum thrust magnitude, throttling factor and velocity vector.

Thrust to mass ratios between 0.05 and 0.08 and burn times between 540 and 750 s are evaluated. The minimum thrust to mass ratio is based on achieving the desired total transfer time. An ideal vacuum specific impulse of 300 s with water as the propellant and a maximum propellant temperature of 1600 K, refer to Figure 2, was used in this analysis. Section 3 provides the propellant selection process where water is selected due to its safety attributes, moderate performance, and high propellant storage density. Figure 3 shows that the shortest burn time to meet the Earth escape time requirement (STP-04) for the lowest thrust to mass ratio is 620 s. For this thrust and burn time combination the resulting total time for the Earth escape maneuver is 2.09 hours with a ΔV of 362.4 m/s and 11 burns. Therefore the spacecraft passes the Van Allen Belts 23 times. The ΔV obtained is about 3 m/s more than the ideal ΔV for the Earth Escape maneuver which corresponds to a total gravity loss of 1% and falls within the assumed 10% margin.

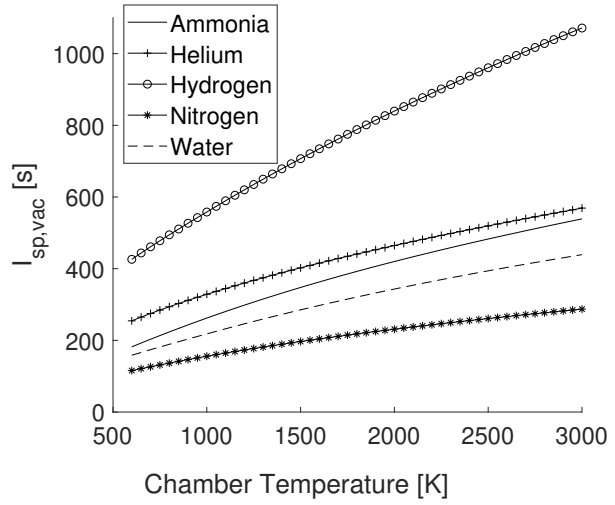

Figure 2. Vacuum specific impulse versus maximum propellant temperature for various propellants. Propellant properties are evaluated with Gasmix fluid model and assume that no dissociation occurs.

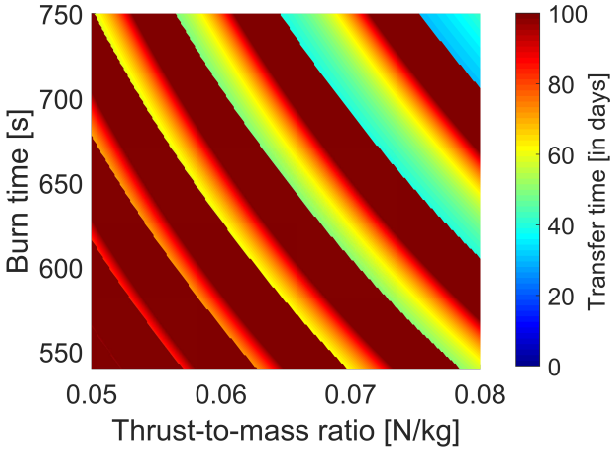

Figure 3. Total transfer time from SSGTO to Earth escape for various thrust-to-mass ratio and burn time combinations.

3. DESIGN STRATEGY

Figure 4 shows a simplified overview of the design process to calculate the mass of the major components of an integrated solar thermal system that combines an STP and ORC system for propulsion and power generation. This section provides design guidelines for future research on evaluating bi-modal solar thermal systems and highlights key challenges based on current technology and limited literature of the system. The integrated solar thermal system is evaluated for the mission described in Section 2 and has been limited to only mini-satellites. Mini-satellites are classified as having a gross mass between 100 and 500 kg. The integrated system can be divided into the following major assemblies: 1) the optical system, 2) the receiver/thermal energy storage (TES) system, 3) the power system, and 4) the propulsion system as shown in Figure 1.

Optical system

Design aspects of the optical system include the selection of the concentrator devices and the concentrator to receiver coupling method. The concentrator devices can either be mirrors or lenses that are rigid or inflatable systems that can be fixed or deployable. For this design a parabolic dish is selected because it has higher concentration ratios compared to spherical mirrors and Fresnel mirrors/lenses and does not suffer from spherical or chromatic aberration [33]. A flat plate secondary concentrator is also selected due to ease of manufacture, simplicity, and compactness versus performance improvement. The concentrator-to-receiver coupling can either be directly coupled or optical fiber cables can be used. The choice of using fiber optic cables is to reduce the pointing accuracy required and decouple the concentrator and receiver position. It has been found that by using many smaller mirrors with fiber optic cables instead of one large mirror the overall system mass can be reduced [34]. The flat plate concentrator also makes it easier to align the fiber bundle and reduces the fiber length. However, the proposed optical system does decrease the end-to-end power efficiency and has higher complexity due to more components with storage integration challenges.

The concentration ratio, CR, determines the maximum temperature the receiver can reach and is defined by Equation 4 as the area of the primary concentrator, A_1, divided by the area of the image which is equivalent to the area of the bundle, A_b. It is also related to the rim angle,ψ_r, the sun half angle, θ_s, and the angular form error, θ_f, as a consequence of machining imperfections. To avoid high fiber transmission losses, the rim angle should be restricted by the fiber's acceptance angle which is dictated by the fiber's numerical aperture. An acceptance angles less than $41.3°$ provide transmission efficiencies greater than 80% [35]. For this study, θ_s is taken as $0.266°$ [36] and no machining imperfections are accounted for and therefore the angular form error is $0°$.

$$CR = \frac{A_1}{A_b} = \frac{\sin^2 \psi_r \cos^2(\psi_r + \theta_s + \theta_f)}{\sin^2(\theta_s + \theta_f)} \tag{4}$$

The mass of the concentrators and support structures can be determined based on areal densities, $\bar{\rho}$, provided in literature, and summarized in Table 4. The fiber mass is determined by the number of fibers, N_f, multiplied by the length of the fiber, L_f, and the linear density, $\bar{m}_f$, of the fiber. The fiber mass per meter is assumed to be 9.95 g/m [37] and the length is assumed to be twice the primary concentrator diameter. This assumption is based on system integration where larger concentrators require more distance from the spacecraft to the receiver to avoid restricting the pointing of the optical system. In this study, inflatable concentrators are used based on their low packaging volume and mass. Therefore an areal density, $\bar{\rho}$, of 1 $\mathrm{kg/m^2}$ is used for the concentrator and 1.5 $\mathrm{kg/m^2}$ is used for the support structures. A conservative value for the support structure is used due to the lack of data available on inflatable support structures. Equation 5 defines the total optical system mass, m_{op}, as being made up of the mass of the primary and secondary concentrator indicated by subscripts 1 and 2 respectively, the support structure and the optical fiber mass, all multiplied by the number of concentrator systems, N_{con}.

$$m_{op} = N_{con}(\bar{\rho}_1 A_1 + \bar{\rho}_2 A_2 + (\bar{\rho}_{\mathrm{sup}} A_1 + \bar{\rho}_{\mathrm{sup}} A_2) + N_f L_f \bar{m}_f) \tag{5}$$

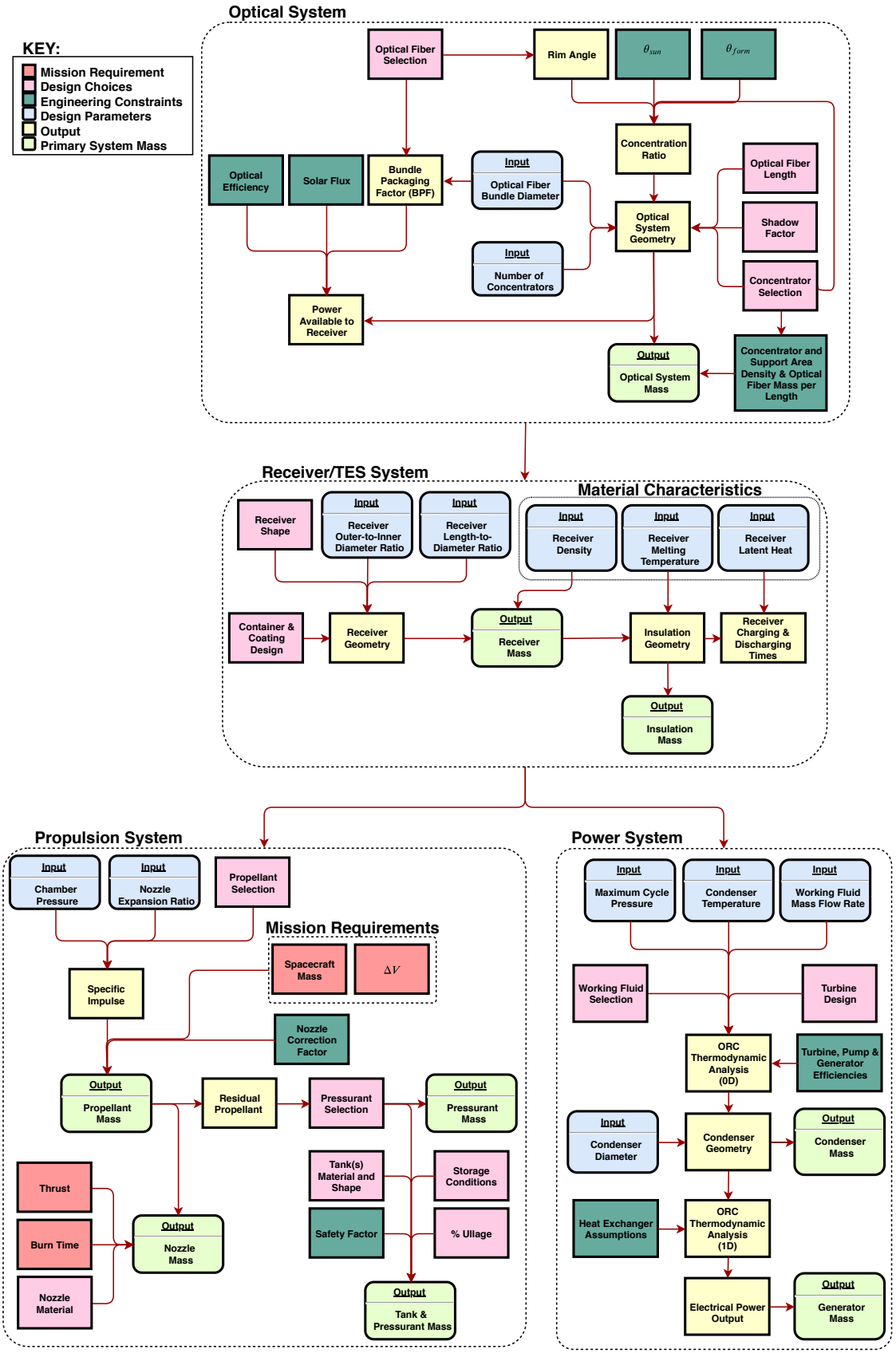

Figure 4. Simplified flowchart of the integrated solar thermal system design process adopted in this paper. Section 3 provides the detailed information of each step and the relevant equations.

Table 4. **Areal densities of existing concentrators and supporting structures**

Structure		Areal Density $[\mathrm{kg/m^2}]$	Ref.
Concentrator	Deployable rigid - ISUS	2.5	[38]
	Deployable rigid - improved manufacturing techniques	1.5	[39]
	Thin film solar concentrators	0.18	[40]
	Inflatbles	< 1	[34, 41]
Support structure	Rigid (for mirror diameters $< 10\ m^2$)	1.5	[15]
	Inflatable	Unknown	

The total input power of the optical system, $\dot{Q}_{in}$, can be calculated using Equation 6,

$$\dot{Q}_{in} = \eta_{op} S N_{op} A_1 \left(1 - b_f\right) \mathrm{BPF} \tag{6}$$

where S is the solar flux, which is assumed to be a constant $1350\,\mathrm{W/m^2}$ during daylight periods of the orbit, and the optical efficiency η_{op} is equal to the combined efficiency of the primary and secondary concentrator and fibers. Concentrator efficiency include reflectivity of the mirrors (90%) and intercept factors (96%) and the fiber efficiency include transmission (90%) and Fresnel efficiency (96.5%) [42]. The bundle packaging factor, BPF, takes into account the packaging efficiency and depends on the fiber selection and the diameter of the bundle (BPF $= N_f A_f / A_b$).

Receiver/TES storage system

Based on the requirement POW-02, the system requires a TES system so that it can operate during eclipse periods. To reduce the number of components and therefore complexity, it is desired to combine the receiver and TES system as a single component. This will also minimize the mass and volume of the overall system. In general, TES systems proposed for STP and or bi-modal solar thermal systems are either sensible or latent heat storage systems. The most common being sensible heating for simplicity and moderate performance. However, this induces large temperature fluctuations. Whereas latent heat storage systems can operate at nearly constant temperatures with high energy storage densities and specific energies that are attractive for future planned interplanetary missions and ORC systems. The major challenges with latent storage systems are the containment issues such as structural integrity and void formation [15]. The shape of the receiver for the preliminary design is restricted to a cylindrical shape to reduce possible stress concentrations by eliminating corners and to easily accommodate the optical fibers entering the receiver aperture. For this study, the receiver is made up of a phase change material (PCM), a container, a coating, and insulation.

The geometry of the receiver depends on the selected shape of the receiver and the receiver's outer-to-inner diameter ratio and length-to-outer-diameter ratio. The inner length of the receiver is assumed to be 80% of the outer length. For all simulations, the receiver is assumed to have a 0.25 mm thick Rhenium coating, with a density of 21,030 $\mathrm{kg/m^3}$ density, a 0.5 mm Boron Nitride container that has a density of 1800 $\mathrm{kg/m^3}$ density. From the geometry and the density of the PCM, container, and coating the mass of the receiver system can be determined.

A one-dimensional steady state radial analysis [43] based on first principles is done to determine the thickness of the insulation for a desired outer insulation temperature. The insulation is divided into four layers and a temperature dependent thermal conductivity is used to improve the accuracy, using carbon bonded carbon fiber[3] as the insulation material. The receiver losses, $\dot{Q}_{loss}$ given by Equation 7, is defined as the summation of the radiation loss though the aperture, $\dot{Q}_{rad}$, the absorption losses of the receiver, $\dot{Q}_{abs}$, and the radiation loss through the insulation, $\dot{Q}_{ins}$. From this and the latent heat of the PCM an estimated charge, t_{ch}, and discharge time, t_{dis}, based on the thermal energy storage of the PCM only can be computed. This is only possible if the energy available per orbit is greater than the energy required by the propulsion system during each burn, the energy required by the ORC system and the energy associated to losses. Due to the preliminary nature, fully charging the TES is assumed to incorporate only the latent heat and not the sensible heat of the PCM and the available input and output powers are assumed to be the steady-state values. Further dynamic investigations are required to determine the operation of the system during a complete orbit and its corresponding transient behavior. The energy fluxes are described by

$$\dot{Q}_{loss} = \dot{Q}_{ins} + \dot{Q}_{rad} + \dot{Q}_{abs} \tag{7}$$

$$\dot{Q}_{rad} = \varepsilon \sigma A_{ap} \left(T_{rec}^4 - T_{space}^4\right) \tag{8}$$

$$\dot{Q}_{abs} = \left[1 - \frac{\alpha_{rec}}{\alpha_{rec} + \left(1 - \alpha_{rec}\right) A_{ap}/A_{in}}\right] \dot{Q}_{in} \tag{9}$$

$$\dot{Q}_{ins} = \varepsilon \sigma A_{ins} \left(T_{ins,o}^4 - T_{space}^4\right) \tag{10}$$

where α_{rec} is the absorptivity of the receiver, ε is the emissivity of the receiver, σ is the Stefan-Boltzmann constant, A_{ap} is the cross-sectional area of the aperture, A_{in} is the inner surface of the receiver, and A_{ins} is the surface area of the insulation. $T_{ins,o}$, T_{rec}, T_{space} are the temperatures of the outside of the insulation, receiver, and environmental temperature respectively. The remaining variables are

$$t_{ch} = \frac{m_{pcm} L}{\dot{Q}_{in} - \dot{Q}_{orc} - \dot{Q}_{loss}}, \text{daylight} \tag{11}$$

[3]**Rigid Carbon Insulation CBCF 15-2000, https://www.mersen.com/products/graphite-specialties/carbon-insulation/rigid-carbon-insulation [Accessed 4 October 2019]**

$$t_{dis} = \frac{m_{pcm} L}{\dot{Q}_{orc} + \dot{Q}_{loss}}, \text{where}$$
$$\dot{Q}_{in} t_{daylight} > \dot{Q}_{orc} t_{orbit} + \dot{Q}_{prop} t_{burn} + \dot{Q}_{loss} t_{orbit} \quad (12)$$

where m_{pcm} is the mass of the PCM, L is the latent heat of the PCM, and $\dot{Q}_{orc}$ is the power required for the ORC system.

A key challenge regarding the complete integrated solar thermal system is the different operating temperatures of the ORC and the STP system. Organic fluids are restricted by their thermal stability limit at around 300 to 400 °C [44–46] and STP desire temperatures above 1000 K to achieve high specific impulse values. This affects the design of the system and thus results in the working fluid tubing being embedded inside the insulation layer if the melting temperature of the receiver material exceeds the thermal limit of the working fluid.

Power system

The on-board electrical power is generated by using an ORC system. The calculation to determine the mass for the major components to meet the desired performance is discussed in this section.

Working fluid selection—The ORC operates by vaporizing the working fluid being passed through a coiled tubing inside the insulation of the receiver. Based on a pre-screening study conducted on 79 potential organic working fluids [5] and a working fluid optimization [7], Toluene is selected as the working fluid. Toluene meets the POW-01 requirement and has been shown to be the optimal fluid in terms of minimizing volume.

Thermodynamic analysis— The preliminary design of the micro-ORC system has been carried out using a Matlab code based on the work of [47]. Fluid thermophysical properties are determined by integrating the code with the software library Fluidprop [48]. The thermodynamic cycle analysis procedure used in this model can be found in [49] and [50]. The condenser was identified as one of the major components in terms of mass for a micro-ORC [7] and is therefore designed in more detail. After the evaluation of the condenser, the ORC thermodynamic analysis is re-evaluated with the calculated pressure drop across the condenser and assumed pressure drops of 1% for the evaporator and both the cold and hot side of the regenerator [7].

Condenser— Heat is radiated to space using a condenser designed with two thin flat sheets of aluminum on the top and bottom coupled to several circular channels. The conductor has a honeycomb support structure in-between, as depicted in Figure 5. The length of the circular channels are discretized into smaller segments and the heat transfer and pressure loss are calculated for each length.

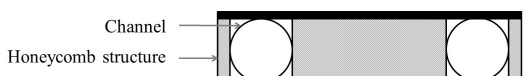

Figure 5. Cross-sectional view of a section of the condenser showing 2 channels, the honeycomb structure and the flat-plate fins.

For the single phase vapor section the laminar and turbulent heat transfer and pressure drop are calculated using the Fanning friction factor and Nusselt number equations in Table 10 provided in the Appendix. For two-phase flow, [51] has identified five flow regimes for condensing flow in microchannels: 1) smooth-annular, 2) wavy-annular, 3) transition, 4) slug, and 5) bubbly. To describe the heat transfer and pressure drop of the condensing section of the channels the universal approach developed by [52,53] has been used due to its large range of applicability. The flow can be characterized with the equations in Table 11 provided in the Appendix where the modified Weber number, We^*, is a parameter that can identify the regime of the condensing flow as either annular or slug and bubbly [54]. The two-phase pressure drop, $(dp/dz)_{tot}$, is made up of the pressure drop due to friction, gravity, and acceleration

$$\left(\frac{dp}{dz}\right)_{tot} = \left(\frac{dp}{dz}\right)_{F} + \left(\frac{dp}{dz}\right)_{G} + \left(\frac{dp}{dz}\right)_{A} \quad (13)$$

where $(dp/dz)_A$ is positive for boiling flow and negative for condensing flow, as the flow decelerates and therefore reduces the pressure drop. For this study, the effects of gravity are neglected, which is acceptable during coasting parts of the mission. The correlations used to determine the frictional and acceleration, in this case deceleration, are provided in the Appendix, Table 13.

The area of the radiator is determined based on the heat-pipe analysis described by [55, Chapter 6] using

$$\dot{Q} = \varepsilon \sigma \eta_e A T_B^4 \quad (14)$$

$$\eta_e = \begin{cases} \left(1 - 1.125\xi + 1.60\xi^2\right)\left(1 - {\theta^*}^4\right), 0.01 \le \xi \le 0.2 \\ \left(-0.405 \log \xi + 0.532\right)\left(1 - {\theta^*}^4\right), 0.2 \le \xi \le 2.0 \end{cases} \quad (15)$$

$$\xi = \frac{\sigma L^2 T_B^3 \left(\varepsilon_1 + \varepsilon_2\right)}{kt} \quad (16)$$

$$\theta^* = \frac{T_s}{T_B} \quad (17)$$

where $\dot{Q}$ is the total radiation power of the condenser-radiator system, T_s is the radiative sink temperature, T_B is the temperature at the fin's base and L is the half length between the channels. The emittance of the top and bottom side of the radiator are indicated as ε_1 and ε_2 respectively, η_e is the fin's effectiveness, k is the thermal conductivity of the fin, and t is the thickness of the fin.

The mass the condenser is therefore the sum of the mass of the working fluid inside the channels (assuming liquid for a more conservative value), the channels, the aluminum fins, the honeycomb core, an adhesive layer and an optical solar reflector (OSR) layer. The mass of the adhesive and OSR layer are determined by their area weight, 0.29 and 0.49 $\mathrm{kg/m^2}$ respectively, multiplied by the top and bottom surface area of the fin. The material volume and density are used to calculate the mass of the remaining components. The density of the channels and fins is 2770 $\mathrm{kg/m^3}$ and the honeycomb is 50 $\mathrm{kg/m^3}$. Support structure and deployment mechanisms have not been considered for simplicity. However, an additional margin of 20% has been included to account for these unknowns.

Generator—Based on a micro-generator survey [7] a linear relationship between the generator mass, m_{gen} and electrical power, $\dot{W}_{net}$ was derived, where the coefficients c_1 and c_2 are defined as 1.8 kg/kW and 2.718 kg,

$$m_{gen} = c_1 \dot{W}_{net} + c_2. \quad (18)$$

Additional components—The regenerator improves the efficiency of the cycle. A crossflow platefin heat exchanger with rectangular channels is chosen due to its lightweight, compactness, and ability to operate at high temperatures. A radial inflow turbine is selected due to its compactness and potential high power density. At these small-scales difficulty in manufacturing occur such as obtaining small blade tip clearances to reduce flow leakage losses. The regenerator, turbine, and tubing have not been included as a compromise of computational design time and the low mass of these components which have been shown to account for less than 1% of the total value [7] and therefore are included in the margin.

Propulsion system

The propulsion system is made up of the propellant, the feed system, and the nozzle.

Propellant selection—Existing theoretical and experimental STP systems have used propellants such as ammonia, helium, hydrazine, hydrogen, nitrogen, and water. Hydrazine is excluded as it does not conform to the STP-05 requirement. Another aspect that needs to be considered is the storability of the propellant for the entire mission duration. Thus, high performing (refer to Figure 2) hydrogen and helium are excluded because although they have a high specific impulse, they have poor storage density and hydrogen suffers from boil-off and therefore not suitable for long-term storage. Nitrogen is suitable to test STP systems but is discarded due to large storage requirements and poor performance, as shown in Figure 2.

From the remaining propellants, ammonia has attractive qualities such as self-pressurising capabilities and higher performance than water. However, water is chosen due to its higher storage density, moderate performance (10% reduction compared to ammonia), and safer attributes regarding health flammability and reactivity. Challenges with using water as a propellant include, potential freezing, thruster corrosion, and the need for a pressurant system.

The specific impulse, I_{sp}, and the propellant mass, m_p, are determined from the mission requirements, ΔV, and spacecraft mass, $m_{s/c}$, and the nozzle correction factor, λ, expansion ratio, ϵ, chamber pressure, P_{ch}, and the temperature of the propellant (taken as T_{melt}). The nozzle expansion ratio, chamber pressure and propellant temperature are design input parameters and are free to vary within a specified range. For simplicity of manufacture a short conical nozzle is assumed with a nozzle correction factor of 96% [56].

$$I_{sp} = \frac{c^* \gamma}{g} \sqrt{\left(\frac{2}{\gamma - 1}\right)\left(\frac{2}{\gamma + 1}\right)^{\frac{(\gamma+1)}{(\gamma-1)}} \left[1 - \left(\frac{P_e}{P_{ch}}\right)^{\frac{(\gamma-1)}{\gamma}}\right]} \tag{19}$$

where c^* is the characteristic velocity, g is the gravitational acceleration ($9.81\,\mathrm{m/s^2}$), γ is the propellant's ratio of specific heats determined at the maximum propellant temperature, and P_e is the exit pressure of the nozzle

$$m_p = m_{s/c}\left(1 - e^{\left(\frac{-\Delta V}{\lambda g I_{sp}}\right)}\right). \tag{20}$$

Feed System—The feed system consists of the propellant tanks, pressurization system, flow lines and valves. Design choices for the tanks include the selection of the material such as composite wrapped, aluminium alloys or titanium, the shape of the tank such as either cylindrical with hemispherical endcaps or spherical and the number of tanks. These choices effect the mass and packaging volume of the system. The tanks are assumed to undergo isentropic expansions due to the relative long burn per maneuver. The GTO-Lunar mission has a high ΔV which results in a large amount of propellant needed which may put constraints on the packaging configuration of the design. Using water requires a pressurant system to be included in the design. In this case, a regulated pressure-fed system is selected as the pressurization system ensures constant operating pressure and therefore thrust, assuming a constant propellant temperature. All the tanks are assumed to be manufactured out of Titanium alloy, Ti-6Al-4V [57]. A single spherical-shaped pressurant tank is assumed and a baseline propellant tank length-to-diameter ratio of 6 is used. To account for pressure losses in the system such as orifices, regulators, and bends and to prevent backflow the propellant tank final pressure is assumed to be twice the chamber pressure. The maximum expected operating pressure (MEOP) is assumed to be 15% more than the design pressure and the burst pressure is 1.5 times the MEOP. To determine the thickness, t, of the tanks (Equation 21) a safety factor, SF, of 2.2 is used that incorporates a 1.2 safety factor over the yield strength, σ_y and an additional safety factor of 2 to account for higher loads and vibration expected during launch [58]. The thickness of the tank, t, is defined as

$$t = \frac{(SF)\,Pr}{(C)\,\sigma_y} \tag{21}$$

where C is the shape constant and is equal to 1 if the tank is cylindrical and 2 if spherical, P is the burst pressure and r is the inner radius of the tank. A minimum wall thickness of 0.5 mm is assumed [59]. For this study, the mass of the flow lines and valves are not included and assumed to be part of the margin.

Nozzle—In this study, a simplified nozzle design was used to calculate the mass of the nozzle in relation to increasing expansion ratio, without considering mission loads such as vibration and the high gas temperature. For this design the divergence angle and convergence angle are assumed to be 15° and 60°. The outer diameter, length, and mass of the nozzle are functions of the chamber pressure, burn time, and expansion ratio.

4. Optimization Set-Up

The objective of this study is to optimize the integrated solar thermal system that could lead to a more competitive design over conventional systems. In this case, the inputs are the ΔV required for the mission, the initial orbit parameters and the mass of the spacecraft. The goal is to minimize the overall wet mass fraction, β, defined as the mass of the bi-modal system, m_{sys}, over the total spacecraft mass, $m_{s/c}$, as shown in Equation 22,

$$\beta = \frac{m_{sys}}{m_{s/c}}. \tag{22}$$

This in turn improves the performance by minimizing the mass of propellant on-board the spacecraft and improving the ORC efficiency by minimizing the concentrator size. The wet system mass is made up of the mass of the optical system, the receiver, the insulation, the propellant, the propellant tank, pressurant, and pressurant tank, the nozzle, and the

condenser. The wet system mass also includes a 20% margin to account for any unknowns and additional components. The amount of time required to fully charge and discharge the PCM which acts as the thermal energy storage (TES) system assuming steady state input and output power operation is constrained to 536 minutes and 104 minutes respectively based on daylight and eclipse periods of a GTO [60]. This is to ensure the system operates during eclipse periods at the initial orbit.

To solve this non-linear problem, a genetic algorithm [61] is implemented to minimize the overall wet mass fraction,

$$\underbrace{F(x)}_{\min} = \beta + \Omega. \tag{23}$$

A penalty, Ω is included if the fluid velocity in the condenser is outside the boundary for liquid, gas, or two-phase flow (Caputo et al., 2011). To ensure the entire design space is investigated the population size and maximum number of generations are set to 130 and 400 respectively. The termination criteria was set as either a convergence criterion of 10^{-10} or the maximum number of generations. An initial mutation rate of 0.02 and a crossover probability of 0.7 are also used. Five spacecraft scenarios were investigated with a gross mass of 100 kg, 200 kg, 300 kg, 400 kg, and 500 kg with an electrical power requirement restricted to 1 W per kg. The five scenarios were analyzed to determine the best sizing of this system for mini-satellites. The chromosome structure is made up of thirteen design parameters which are discussed next.

Design Parameters

A total of thirteen design variables have been identified to analyze the design of the proposed integrated solar thermal system and determine the mass of the major components of the system.

1. **Number of concentrators:** The number of concentrators effects both the energy input of the system and the mass of the concentrators. Increasing the number of concentrators requires more optical fiber bundles and thus effects the inner diameter of the receiver and therefore increases the radiation losses due to an increase in receiver surface area. The minimum number of concentrators is required to ensure adequate power into the system so that the thermal energy storage can discharge over the entire eclipse period.
2. **Optical fiber bundle diameter:** The diameter of the bundle is made up of the maximum number of fiber optic cables to fit within a circle. Each optical fiber is assumed to be 1.3 mm, with a numerical aperture of 0.66 [34]. Due to the circular shape of the fibers the total area of the bundle is not useful and this is accounted for by defining the bundle packaging factor. Although [62] discusses the possibility of polishing the fiber tips to obtain a bundle packaging factor close to 1. The diameter of the concentrator is constrained by the numerical aperture, NA, of the optical fiber and the diameter of the bundle, Equation 24. Increasing the bundle diameter therefore increases the mass of the concentrator, receiver and insulation. A minimum TES charge time is possible as a compromise between the decrease in charging time due to the increase in input power and the increase in charging time due to the increase of the receiver mass. The numerical aperture is defined as

$$NA = n_e \sin \psi_a \tag{24}$$

where n_e is the external refractive index and ψ_a is the acceptance angle of the optical fiber cable. The rim angle of the concentrator is constrained to equal the acceptance angle to minimize fiber transmission losses.
3. **Receiver outer-to-inner-diameter ratio:** To design the receiver an outer-to-inner-diameter ratio is assumed as a design parameter and this has a direct effect on the mass of the receiver and insulation as well as the energy storage charging and discharging time of the system.
4. **Receiver length-to-diameter ratio:** The length-to-diameter ratio of the receiver also effects the shape of the receiver and therefore the mass and storage capability of the receiver.
5. **Receiver melting temperature:** The melting temperature of the PCM significantly effects the propellant temperature and thus specific impulse. It also results in higher radiation losses which increases the insulation thickness. A minimum mass exists as a compromise between the reduction in propellant mass and therefore lighter feed system (tank, and pressurant system) and nozzles against the increase in insulation mass. The position of the ORC channel is also affected by the PCM temperature. Increasing the melting temperature of the receiver, in other words increasing the final propellant temperature increases the power required to vaporize the propellant therefore increasing the charging and decreasing the discharging time respectively.
6. **Receiver density:** To evaluate a number of different materials the density of the PCM is provided as an input. The density directly proportionally affects the mass and therefore charging and discharging times of the TES.
7. **Receiver latent heat:** Another characteristic of the PCM is the latent heat. The latent heat has no direct effect on the mass of the system but it is directly proportional to the charging and discharge time.
8. **Thruster expansion ratio:** By increasing the nozzle expansion ratio, the specific impulse can be improved, which reduces the mass of propellant and feed system (tank and pressurant). However at a cost of a heavier nozzle therefore an optimal minimum mass exists. Longer nozzles also result in larger losses, although in this optimization study the nozzle losses were kept constant, therefore a balance also exists between better expansion ratios and larger losses. Investigation into the effect of varying the nozzle correction factor is provided in Section 6.
9. **Chamber pressure:** High chamber pressures effects the structural sizing by requiring thicker walls for the tubing as well as the tanks and other upstream components which require to be at a higher pressure. The larger wall thickness result in an increase of the overall mass. However, the benefit of higher chamber pressures is the reduction in nozzle mass as the throat area is inversely proportional to the chamber pressure. An optimal minimum mass exist between the increase in feed system mass and decrease in nozzle mass.
10. **ORC maximum cycle pressure:** The maximum cycle pressure effects the structural sizing of the turbine but also the rotational speed and rotor blade height of the system which influence the feasibility of the system with current bearing technology and manufacturing limitations. It should be noted that with current manufacturing limitations, the minimum acceptable rotor blade height should be 0.2 mm [7]. The increase in maximum cycle pressure improves the thermal efficiency of the system and thus the electrical power output. This increases the mass of the generator due to the derived linear relationship (Equation 18). The condenser mass also increases as the temperature entering the condenser is hotter for higher cycle pressures. Therefore the area of the condenser has to increase to accommodate the higher enthalpy change. Higher cycle pressures would also increase the tubing mass of the ORC system, however, this has not been considered in this study. The increase in electrical power

output results in the charge time increasing and the discharge time decreasing.

11. **ORC mass flow rate:** The working fluid mass flow rate directly effects the net electrical power output of the ORC system and therefore the mass of the generator. The condenser mass also increases for larger mass flow rates due to the larger condensation power required.

12. **Condenser temperature:** Increasing the temperature of the condenser reduces the thermal efficiency of the ORC system and therefore reduces the charge time and increases the discharge time of the TES system. However, higher condenser temperature values result in a larger temperature difference between the external temperature of the condenser, which acts as a radiator, and the space environment temperature which effects the amount of radiation that can be expelled from the system and therefore the size of the radiator.

13. **Condenser diameter:** The diameter of the condenser effects the mass flux inside the flow channels of the condenser which directly affects the pressure drop of system and therefore the mass of the condenser. Due to the discrete nature of the number of channels of condenser (constrained to be the maximum number of channels based on velocity boundary guidelines of single and two-phase flow in pipes [63]), variations in the diameter results in discrete changes in the mass, electrical power output, charge time, and discharge time.

5. Sensitivity Analysis Set-Up

Sensitivity analyses on the design parameters, design choices, and constant parameters were conducted to identify the influence of the variables on the integrated solar thermal design.

Design parameters—From the optimization study a baseline design is obtained for the 500 kg satellite scenario. The design parameters were evaluated between $\pm 30\%$ from the baseline values using a one-at-a-time method to evaluate their corresponding effect on the wet mass of the system. The number of concentrators parameter was constrained to integer values only.

Design choices—An additional sensitivity analysis to evaluate the effect of certain design choices on the overall wet mass fraction has also been conducted. Here, the focus is on design choices such as the number of tanks and thrusters as well as the shape of the propellant tank and the desired outer temperature of the insulation layer. The boundary defined for these parameters are based on packaging arrangements of the propellant tank, the thrust vectoring capability of the spacecraft, and the requirements of the internal temperature of the spacecraft. The optical fiber diameter and the optical fiber NA, which relates to the primary concentrator's rim angle, are also analyzed. The boundary for these parameters are based on commercially available optical fibers. The baseline design for this analysis is again the optimized solution for the 500 kg satellite scenario. Table 5 provides the design choice parameters used in this study.

Uncertainty— An Analysis of variance (ANOVA) was performed to assess the influence of the uncertain parameters in the system model to identify critical parameters. The outputs analyzed are the overall wet mass fraction, the electrical power, and the charging and discharging time of thermal energy storage system. The percentage contribution or variable importance, which indicates the influence magnitude of a parameter on the outputs, is defined as the sum of squares of each factor divided by the total sum of squares. Parameters under investigation include the optical, turbine, pump, and generator efficiency. The nozzle correction factor, condenser pinch point temperature, and the radiating space environment temperature that the condenser is exposed too are also evaluated. The maximum and minimum range of all these variables are given in Table 6. Predicted optical efficiency ranges for current and space-based deigns are provided by [42]. Literature, although focused on larger Rankine systems, provide an estimation for the expected turbine, pump, and generator efficiency range [18, 64]. Condenser pinch point temperature range is assumed to be between 10 and 30 to cover a large range of operation conditions. Deep-space temperature is taken as 4 K and is the lower limit of the environmental temperature the condenser radiates too, however depending on the position of the satellite the condenser may be exposed to higher temperatures due to sunlight, planetary infrared, and albedo effects. An upper limit of 300 K is based on assuming the condenser radiates to the satellite surface which is equivalent to 300 K at 1 AU from the Sun. The nozzle correction factor range is based on reducing the nozzle losses from the current conical-shape nozzle by using a bell-shape nozzle which can achieve correction factors up to 99% [56].

6. Results and Discussion

Validation

To ensure fidelity of the models, a number of validations have been conducted. The concentrator is one of the largest components of the system and therefore it is important to ensure the sizing is properly modeled. Table 7 presents the results of this study against the works of [65] and [66] and falls within an acceptable range. The large deviation of 17% for the stowed volume is due to the limited information of the 0.5 m dish design from [66] and that this study assumes the rigid volume is a cylinder. The work of [15] has been used to validate the sizing of the phase change receiver model. The results fall within a 2% difference. The discrepancy is possibly due to a difference in densities used. The condenser validation assumed a two sided flat aluminum heat pipe radiator that operates at $21^{\circ}\mathrm{C}$ with a sink temperature of $-87^{\circ}\mathrm{C}$, the heat pipe mass per meter is 0.11 kg/m and 1000 W is required to be radiated. The analysis was conducted for a range of fin thickness values (0.18 to 0.5 mm) and pipe spacings (0.1 to 0.3 cm) with the results showing an average difference less than 3%. All models, except for the volume of the optical system, are within the acceptable threshold of 5%. The large 17% deviation of the volume concentrator model is still acceptable due to the more conservative approach taken in this work. The storage volume of the concentrator is also assumed to be inflatable which is linked to the concentrator's areal density taken from literature.

Optimization results

Figure 6 provides the final optimization solution of the wet mass fraction for each scenario investigated. The results show that the proposed integrated solar thermal system is better suited to larger mini-satellites as they have lower overall mass fractions. For the scenarios that have a spacecraft mass of 200 kg and less, the system requirement SYS-01 is not met. The 400 kg and 500 kg are the most suited for the GTO-Lunar mission as they have a mass fraction close to 75% which could compete with conventional systems [31]. Using tanks that are composed of a combination of titanium and composite materials could further reduce the mass fraction of the existing design to make it more competitive. The larger designs also result in fewer number of concentrators

Table 5. Design choice sensitivity analysis input parameters

		Parameter values for Figure 9										
		a	**b**	**c**	**d**	**e**	**f**	**g**	**h**	**i**	**j**	**k**
Fiber diameter	[mm]	1	1,3	2	4	6	8	10	12	14		
Rim angle	[°]	12.70	15.56	18.42	21.28	24.14	27.00	29.80	32.72	35.58	38.44	41.30
Insulation temperature	[K]	350	400	450	500	550	600					
# thrusters	[-]	1	2	3	4							
# tanks	[-]	1	2	3	4							
Tank L/D ratio	[-]	1	2	3	4	5	6	7	8	9	10	

Table 6. Uniform distribution of parameters for the uncertainty sensitivity analysis

Parameter	Range
Optical efficiency [%]	[55-85]
Turbine efficiency [%]	[50-80]
Pump efficiency [%]	[30-60]
Generator efficiency [%]	[80-95]
Condenser pinch point temperature [K]	[10-30]
Condenser environment temperature [K]	[4-300]
Nozzle correction factor [%]	[96-99]

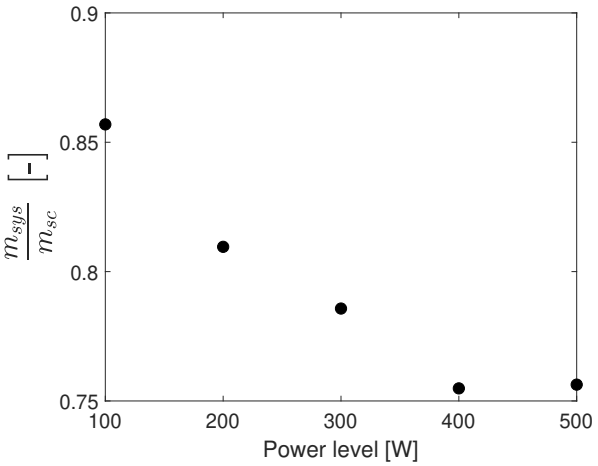

Figure 6. Final optimal solution of the wet mass fraction of the propulsion and power system for the five scenarios.

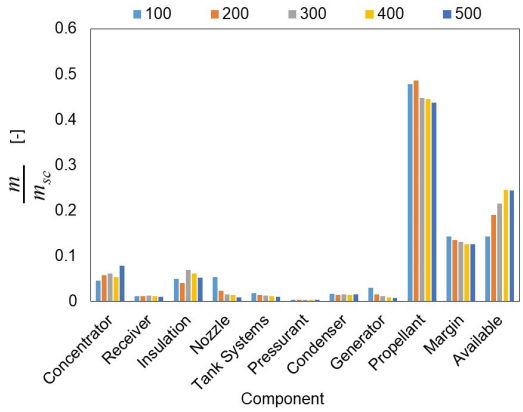

Figure 7. Normalized mass of all the major components for the five scenarios.

and therefore would reduce complexity by employing simpler deployment and tracking systems. Table 8 provides the optimal design parameters for all the scenarios and indicates the baseline used for the sensitivity analyses.

The PCM design parameters results in Table 8 show a melting temperature, density, and latent heat range of 1500 to 2000 K, 1800 to 3000 $\mathrm{kg/m^3}$, and 4600 to 5000 kJ/kg respectively. Silicon and boron are existing PCM that best fit these ranges with silicon not meeting the latent heat range and the boron slightly exceeding the melting temperature range, refer to Table 9 [15, 65, 67, 68]. These materials meet the future planned interplanetary specific energy target of greater than 250 Wh/kg. The design chamber pressure is between 4 and 5 bar for all the scenarios. Taking into consideration the concentrator, generator, condenser and 20% margin the estimated power density is between 8 and 11 W/kg for the five scenarios.

The mass distribution of the optimal solutions of the five mini-satellite scenarios illustrated in Figure 7, shows the propellant mass accounts for between 40% and 50% of the total mass. The normalized propellant mass is dependent on the melting temperature of the optimal solution, and therefore why the 200 kg scenario shows the highest value as it has the lowest melting temperature. The concentrator and insulation are the next heaviest components contributing up to 8% of the total mass. The condenser and receiver account for approximately 1.5% and 1% of the total mass regardless of the spacecraft size. The nozzle, tanks system and generator normalized mass decreases with increasing spacecraft size.

Sensitivity analysis results

Design parameter— The number of concentrators and the diameter of the bundle (optical parameters) have the most influence on the mass fraction with a change from the baseline value of up to 18.2% and 12.3% respectively (Figure 8). Increasing the optical design parameters causes the diameter of the primary concentrator and the aperture of the receiver to increase. This increases the mass of the concentrator, receiver and insulation. The receiver outer-to-inner diameter has the third largest effect with a maximum of 7.5% deviation from the baseline value. The receiver and insulation mass are directly proportional to the outer-to-inner diameter of the receiver. The melting temperature of the PCM results in an optimal minimal point as a compromise between the increase in insulation mass and the decrease in propellant, tank, pressurant, and nozzle mass. For this sensitivity analysis, the other design parameters have an effect of less than 2% on the mass fraction.

Table 7. Model validation results

System	Parameter	Unit	Reference Value	Reference	This Study	Difference [%]
Receiver						
	PCM Mass	[kg]	66.8	[15]	67.3	0.7
	Container Mass	[kg]	9.4	[15]	9.3	1.1
	Coating Mass	[kg]	62.6	[15]	52.4	0.4
	Total Mass	[kg]	128.8	[15]	129	0.2
Optical						
	Focal Length	[mm]	33.7	[65]	33.8	0.3
	Mass	[kg]	15	[65]	14.78	1.5
	Rigid Volume	$[m^3]$	0.05	[66]	0.0593	17
Condenser						
	Average Area	$[m^2]$	5.24	[55]	5.16	1.4
	Average Mass	[kg]	3.76	[55]	3.67	2.9

Table 8. Final optimized design parameters for each mini-satellite scenario

S/C mass	D_b	D_o/D_i	L/D	ε	P_c	T_{melt}	ρ	L	$\dot{m}$	P_{max}	T_{cd}	D_{cd}	N_{conc}
100	3	37.6	18.7	226	4.89	1550	2946	4839	1.14	31.78	115	2.03	19
200	5	28	27.7	193	4.76	1501	2768	4970	2.95	33.9	142	2.17	16
300	7	33.0	19.4	172	4.21	1851	2462	4744	5.05	21.04	144	6.21	12
400	7	36.4	16.8	221	4.57	1849	1844	4938	5.63	31.15	139	5.15	14
500 (*baseline*)	14	33.8	9.7	166	4.37	1964	2785	4617	6.78	26.69	129	3.68	5

Table 9. Properties of high-temperature Silicon and Boron phase change materials

Material	Melting Temperature [K]	Latent Heat [kJ/kg]	Density [kg/m^3]	Specific Energy [Wh/kg]
Boron	2350	4600	2350	1278
Silicon	1687	1785	2580	496

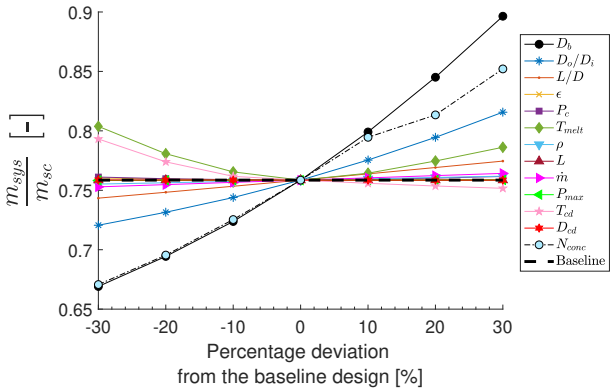

Figure 8. Sensitivity results of the design parameters.

Design choice—The results in Figure 9 show that the parameters with the largest effect on the overall wet mass fraction are the desired insulation temperature and the fiber diameter. The variation of these parameters from the baseline value are 7.9% and 5.3% respectively. By increasing the desired insulation temperature, the insulation thickness can be reduced resulting in a significant reduction in insulation mass. Increasing the fiber diameter improves the BPF except for the 10 mm and 12 mm case which reduced the BPF such that the energy into the receiver is less than the energy required for the propulsion, power, and losses. These infeasible solutions are indicated in Figure 9 by the dash-lines. When increasing the fiber diameter, the mass of the bundle reduces as the number of fibers reduce which decreases the mass of the optical system. The fiber mass per length was adjusted such that it increased for increasing diameters based off a reference diameter. The rim angle can also significantly effect the overall mass fraction. The rim angle which is determined based on the optical fibers numerical aperture is directly proportional to the primary diameter of the concentrator and therefore the available input power. At low values, the energy in is less than the energy required by the system. Spherical tanks, as expected, produces the lowest overall mass fraction, however a cylindrical tank with a length-to-diameter ratio of 5 provides the best gain in mass saving to increasing ratios. Depending on the restriction of packaging the propellant tank inside the spacecraft, the overall system mass is only increased by 0.9% by increasing the number of propellant tanks from 1 to 4. Lastly, by increasing the number of thrusters the total nozzle mass reduces (by 0.4%) due to the decrease of the throat and exit diameter caused by the decrease in thrust per thruster. Increasing the number of thrusters is also beneficial for propulsion redundancy and can assist with misalignment correction by controlling the mass flow rate of each valve.

Uncertainty—The three constant parameters that influence the overall wet mass fraction of the system the most are the condenser pinch point temperature, the nozzle correction factor, and the environmental temperature exposed to the con-

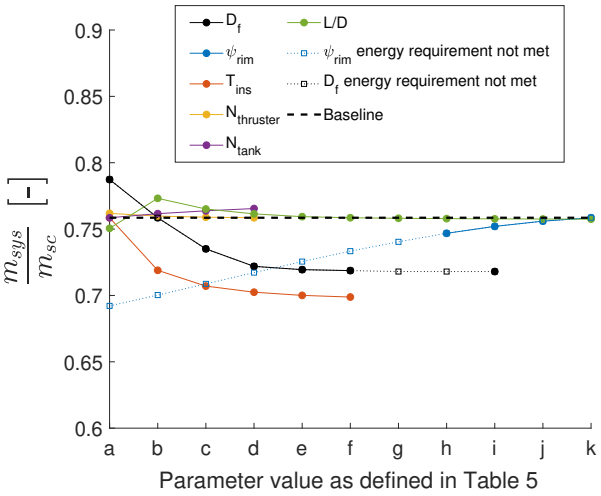

Figure 9. **Sensitivity results of the design choices.**

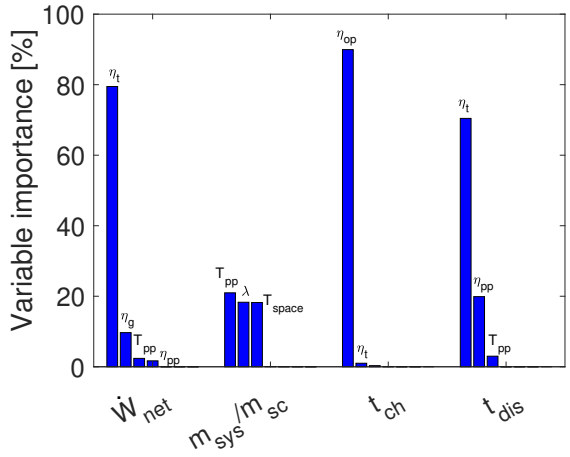

Figure 10. **Percentage contribution of the uncertain parameters for the integrated solar thermal model.**

denser. Figure 10 indicates that these parameters can effect the response up to approximately 20%. The condenser pinch point temperature which is taken as the difference between the saturated temperature and the wall temperature of the condenser has the largest influence. Higher condenser pinch point values reduce the wall temperature of the condenser and therefore increase the required area and thus mass of the condenser. Experimental testing of the thruster can be conducted to evaluate the nozzle losses and to minimize the losses which will result in high-performing low mass nozzles. A more detailed condenser model that evaluates the condenser in the space environment and accounts for albedo effect and the position of the condenser versus the Sun and Earth would be able to predict more accurate results on the temperature of the condenser and space environmental temperature per orbit to determine a more accurate range.

The isentropic efficiency of the turbine has the largest effect of almost 80% on the output electrical power, indicated in Figure 10. This identifies the need to more accurately predict the losses of micro-turbines. Currently, existing loss models and experimental testing are limited to larger-scale designs and often do not include organic fluids. Future work will need to evaluate the turbine efficiency of a micro-turbine using available large-scale models to determine possible range to improve confidence level. Then, attempts to improve the confidence level by improving the existing loss models to account for small-scale application will be investigated. Experimental testing is also necessary to verify predictions.

Regarding the charging time of the TES system, the optical efficiency contributes to largest variation of up to 90%. The optical efficiency is directly proportional to the input power of the concentrator which is inversely proportional to the charge time (Equation 11). The discharge time is inversely proportional to the output power of the system which includes the electrical power output, Equation 12. Therefore, the turbine efficiency and pump efficiency are the main variables that contribute to the variation. The turbine is largest due to the larger boundary of efficiency evaluated due to the higher uncertainty of this variable.

7. SUMMARY

The study focuses on a novel design of an integrated solar thermal system that can generate electricity with a micro-ORC system that uses the waste energy from a solar thermal propulsion system. The design uses water as the propellant and toluene as the working fluid. This proposed design was evaluated as a possible alternative for a Lunar orbit insertion mission. A single objective optimization was conducted using a genetic algorithm to minimize the overall wet system mass fraction. The optimization results illustrate that for the GTO to Lunar mission the integrated solar thermal system is most suitable for satellites that have a gross mass of 400 kg or more.

It was found that a PCM material with a density between 1800 and 3000 $\mathrm{kg/m^3}$, a latent heat between 4600 and 5000 $\mathrm{kJ/kg}$, and a melting temperature between 1500 and 2000 K is desired. Silicon and boron are therefore potential PCM candidates that could be used at a sacrifice of latent heat or melting temperature respectively. Both these materials can provide specific energies greater than the 250 Wh/kg desired for future planned interplanetary missions. Regarding the mass distribution of the integrated design the propellant mass accounts for 40 to 50% of the total mass fraction. The next heaviest components of the design are the concentrator and insulation which contribute 8% of the total mass. The disadvantage however, is low power densities of around 10 W/kg. Attractive features of the integrated system are high specific energy, fast transfer times, higher resistance to degradation, and a propulsion system with lower power consumption compared conventional systems and potentially lower cost.

The optical parameters have the largest influence on the the overall system mass fraction of up to 18.2% and the outer-to-inner receiver diameter ratio has more effect than the length-to-diameter ratio. An optimal minimum mass exists for the PCM melting temperature design variable as there is a compromise between the increase in insulation mass and the reduction in propellant, pressurant, and tank mass. Additional design considerations are that unless the packaging of spherical tank can be accommodated a tank length-to-diameter of 5 is found to be the most suitable with regards to mass saving. The desired outer temperature of the insulation has a significant effect of up to 7.9% on the overall mass fraction. Optical fibers with high rim angle are required to ensure adequate input power is received. The selection of the fiber diameter needs to ensure a high bundle packaging

factor depending on the diameter of the bundle required to minimize the overall mass. An investigation on the influence on constant parameters show that the isentropic efficiency and optical efficiency drive the electrical power output and charging time. The results vary with design assumptions, and the fidelity of the model. For more reliable data, the complexity of the mass estimation models for the concentrator, water tank blowdown, insulation, and condenser design can be increased.

Future work will include investigating the losses of a microturbine in more detail to better predict the turbine isentropic efficiency as well as dynamic modeling of the receiver and fluid coupling. Testing inflatable concentrator systems to provide better optical efficiency values and modeling the dynamic response of the integrated system focusing on the receiver-fluid interaction are also recommended.

APPENDIX

Tables 10, 11 and 13 provide the equations used to determine the heat transfer coefficient, h and the pressure drop dp/dz in the condenser for single and two-phase flow. Two-phase flow variables are indicated with the subscript, *tp*.

REFERENCES

[1] R. Surampudi, J. Blosiu, P. Stella, J. Elliott, J. Castillo, T. Yi, J. Lyons, M. Piszczor, J. McNatt, C. Taylor, E. Gaddy, S. Liu, E. Plichta, and C. Iannello, "Solar Power Technologies for Future Planetary Science Missions," NASA, Pasadena, Califronia, Tech. Rep., 2017.

[2] R. Surampudi, J. Blosiu, R. Bugga, E. Brandon, M. Smart, J. Elliott, J. Castillo, T. Yi, L. Lee, M. Piszczor, T. Miller, C. Reid, C. Taylor, S. Liu, E. Plichta, and C. Iannello, "Energy Storage Technologies for Future Planetary Science Missions," NASA, Pasadena, Califronia, Tech. Rep., 2017.

[3] M. D. Antonio, C. Shi, B. Wu, and A. Khaligh, "Design and Optimization of a Solar Power Conversion System for Space Applications," *IEEE Transactions on Industry Applications*, 2019.

[4] K. Montgomery, J. Buckner, Z. Levin, J. Cromer, and D. Wilt, "Advanced Space Power Technology Development at the Air Force Research Laboratory," in *AIAA Scitech 2019 Forum*, 2019, p. 1671.

[5] F. Leverone, A. Cervone, M. Pini, E. Gill, and P. Colonna, "Feasibility of an integrated solar thermal power and propulsion system for small satellites," in *Proceedings of the International Astronautical Congress, IAC*, vol. 13, 2017.

[6] F. Leverone, A. Cervone, and E. Gill, "Cost analysis of solar thermal propulsion systems for microsatellite applications," *Acta Astronautica*, vol. 155, pp. 90–110, 2019.

[7] F. Leverone, M. Pini, A. Cervone, and E. Gill, "Feasibility of an On-board Micro-ORC System for Small Satellites," in *5th International Seminar on ORC Power Systems*, Athens, 2019.

[8] R. M. Zubrin, T. K. Sulmeisters, M. G. Jacox, and K. Watts, "The integrated power and propulsion stage: A mission driven solution utilizing thermionic technology," in *AIP Conference Proceedings*, vol. 246, 1992, pp. 1259–1267.

[9] K. K. Laug, M. R. Holmes, and K. O. Westerman, "Solar Bi-modal system concept: Mission applications, a preliminary assessment," in *AIP Conference Proceedings*, vol. 324, no. 1, 1995, pp. 155–159.

[10] K. K. Laug, M. Holmes, K. O. Westerman, and R. Spickard, "Solar bi-modal system concept: Common development issues with nuclear systems," in *AIP Conference Proceedings*, vol. 324, no. 1, 1995, pp. 821–826.

[11] J. Malloy, R. Rochow, and J. Inman, "Hybrid Solar Rocket Utilizing Thermal Storage for Propulsion and Electrical Power," Patent and Trademark Office, US Patent 5,459,996, 1995.

[12] P. Frye, "Integrated solar upper stage (ISUS) space demonstration design," in *Space technology and applications international forum (STAIF - 97)*. ASCE, 1997, pp. 461–466.

[13] C. T. Kudija and P. E. Frye, "Integrated Solar Upper Stage (ISUS) engine ground demonstration (EGD)," in *AIP Conference Proceedings*, vol. 420, no. 1, 1998, pp. 348–353.

[14] T. L. Kassler, P. Frye, and R. Partch, "Solar thermal OTV - Applications to reusable and expendable launch vehicles," *Acta Astronautica*, vol. 47, no. 2-9, pp. 215–226, 2000.

[15] M. Gilpin, "High Temperature Latent Heat Thermal Energy Storage to augment Solar Thermal Propulsion for Microsatellites," Ph.D. dissertation, University of Southern California, 2015.

[16] A. K. Hyder, R. L. Wiley, G. Halpert, D. J. Flood, and S. Sabripour, *Spacecraft power technologies*. Imperial College Press London, 2000, vol. 1.

[17] M. Gilpin, D. B. Scharfe, M. Young, and A. Pancotti, "Molten boron phase-change thermal energy storage: containment and applicability to microsatellites," in *42nd AIAA Thermophysics Conference*, 2011.

[18] G. Angelino, C. Invernizzi, and E. Macchi, "Organic working fluid optimization for space power cycles," in *Modern research topics in aerospace propulsion*. Springer, 1991, pp. 297–326.

[19] D. Schubert, "Mems-concept using micro turbines for satellite power supply," in *Solar Power*. InTech, 2012, ch. pp.195-210.

[20] N. Muller and L. G. Fréchette, "Performance analysis of Brayton and Rankine cycle microsystems for portable power generation," in *ASME 2002 International Mechanical Engineering Congress and Exposition*. American Society of Mechanical Engineers, 2002, pp. 513–522.

[21] G. Angelino and C. Invernizzi, "Cyclic methylsiloxanes as working fluids for space power cycles," *Journal of solar energy engineering*, vol. 115, no. 3, pp. 130–137, 1993.

[22] J. Harinck, P. Colonna, A. Guardone, and S. Rebay, "Influence of thermodynamic models in two-dimensional flow simulations of turboexpanders," *Journal of turbomachinery*, vol. 132, no. 1, p. 11001, 2010.

[23] A. Uusitalo, T. Turunen-Saaresti, A. Guardone, and A. Grönman, "Design and flow analysis of a supersonic small scale ORC turbine stator with high molecular complexity working fluid," in *ASME Turbo Expo 2014: Turbine Technical Conference and Exposition*. American Society of Mechanical Engineers, 2014, pp. V03BT26A004–V03BT26A004.

Table 10. **Fanning friction factors used in the condenser and evaporator model for single phase flow**

Flow regime	Equations	Condition
Laminar	$f_k = \frac{16}{\mathrm{Re}_k}$ $\mathrm{Nu_k} = 4.364$	$\mathrm{Re}_k < 2000$
Turbulent	$f_k = \frac{0.079}{\mathrm{Re}_k^{0.25}}$	$2000 \leq \mathrm{Re}_k < 20,000$
	$f_k = \frac{0.046}{\mathrm{Re}_k{}^{0.2}}$	$\mathrm{Re}_k \geq 20,000$
	$\mathrm{Nu_k} = \frac{\left(\frac{\mathrm{f_k}}{2}\right)(\mathrm{Re_k}-1000)\,\mathrm{Pr_k}}{1+\left[12.7\left(\frac{\mathrm{f_k}}{2}\right)^{0.5}\left(\mathrm{Pr_k}^{\frac{2}{3}}-1\right)\right]}$	$0.5 \leq \mathrm{Pr}_k \leq 2000, 2300 \leq \mathrm{Re_k} \leq 5\times10^6$

where the subscript k stands for either liquid, f, or vapour, g.

Table 11. **Heat transfer correlations for condensing flow in mini channels**

Two-phase flow regime
Annular flow (smooth-annular, wavy-annular, transition), where $\mathrm{We}^* > 7\mathrm{X_{tt}}^{0.2}$ $h_{tp} = \frac{k_f}{D_{hyd}} 0.048 \mathrm{Re}_f^{0.69}\,\mathrm{Pr}_f^{0.34}\,\frac{\phi_g}{X}$
Slug and bubbly flow, where $\mathrm{We}^* < 7\mathrm{X_{tt}}^{0.2}$ $h_{tp} = \frac{k_f}{D_{hyd}}\left[\left(0.048\mathrm{Re}_f^{0.69}\,\mathrm{Pr}_f^{0.34}\,\frac{\phi_g}{X}\right)^2 + \left(3.2\times10^{-7}\mathrm{Re}_f^{-0.38}Su_{go}^{1.39}\right)^2\right]^{0.5}$
The modified Weber number We^* is defined by [69] as $\mathrm{We}^* = 2.45\frac{\mathrm{Re_g}^{0.64}}{\mathrm{Su_{go}}^{0.3}(1+1.09\mathrm{X_{tt}}^{0.039})^{0.4}}$, for $\mathrm{Re}_f \leq 1250$ $\mathrm{We}^* = 0.85\frac{\mathrm{Re_g}^{0.79}\mathrm{X_{tt}}^{0.157}}{\mathrm{Su_{go}}^{0.3}(1+1.09\mathrm{X_{tt}}^{0.039})^{0.4}}\left[\left(\frac{\mu_\mathrm{g}}{\mu_\mathrm{f}}\right)^2\left(\frac{\mathrm{v_g}}{\mathrm{v_f}}\right)\right]^{0.084}$, for $\mathrm{Re}_f > 1250$
Additionally the superficial liquid Reynolds number, Re_f, and the Lockhart-Martinelli parameter, X_{tt}, are defined as $\mathrm{Re}_f = \frac{G(1-x)D_{hyd}}{\mu_f}$. $X_{tt} = \left(\frac{\mu_f}{\mu_g}\right)^{0.5}\left(\frac{1-x}{x}\right)^{0.5}\left(\frac{\rho_g}{\rho_f}\right)^{0.5}$, where, $\phi_g^2 = 1 + CX_1 + {X_1}^2$, refer to Table 12 for the determining constant, C, $X_1 = \frac{(dp/dz)_f}{(dp/dz)_g}$, $-(dp/dz)_f = \frac{2f_f G^2(1-x)^2}{D_{hyd}\rho_f}$, $-(dp/dz)_g = \frac{2f_f G^2 x^2}{D_{hyd}\rho_g}$.

Table 12. **Constant correlations used to determine the Lockhart-Martinelli two-phase pressure drop multiplier, ϕ**

Liquid	Vapour	Constant C	Reynolds Number
Turbulent	Turbulent	$C = 0.39\mathrm{Re}_{fo}^{0.03}Su_{go}^{0.10}\left(\frac{\rho_f}{\rho_g}\right)^{0.35}$	$\mathrm{Re}_f \geq 2000, \mathrm{Re}_g \geq 2000$
Turbulent	Laminar	$C = 8.7\times10^{-4}\mathrm{Re}_{fo}^{0.17}Su_{go}^{0.50}\left(\frac{\rho_f}{\rho_g}\right)^{0.14}$	$\mathrm{Re}_f \geq 2000, \mathrm{Re}_g < 2000$
Laminar	Turbulent	$C = 0.0015\mathrm{Re}_{fo}^{0.59}Su_{go}^{0.19}\left(\frac{\rho_f}{\rho_g}\right)^{0.36}$	$\mathrm{Re}_f < 2000, \mathrm{Re}_g \geq 2000$
Laminar	Laminar	$C = 3.5\times10^{-5}\mathrm{Re}_{fo}^{0.44}Su_{go}^{0.50}\left(\frac{\rho_f}{\rho_g}\right)^{0.48}$	$\mathrm{Re}_f < 2000, \mathrm{Re}_g < 2000$

Table 13. **Two-phase flow pressure drop equations**

Pressure drop type	
Acclerational pressure drop	
$-\left(\frac{dp}{dz}\right)_A = G^2 \frac{d}{dz}\left[\frac{x^2}{\alpha\rho_g} + \frac{(1-x)^2}{(1-\alpha)\rho_f}\right]$	
$\alpha = \left[1 + \left(\frac{1-x}{x}\right)\left(\frac{\rho g}{\rho_f}\right)^{2/3}\right]^{-1}$	[70]
Frictional pressure drop	
$\left(\frac{dp}{dz}\right)_F = \left(\frac{dp}{dz}\right)_f \phi_f^2 = \left(\frac{dp}{dz}\right)_g \phi_g^2$	

[24] A. M. Cipriano, D. A. Dei Tos, and F. Topputo, "Orbit Design for LUMIO: The Lunar Meteoroid Impacts Observer," *Frontiers in Astronomy and Space Sciences*, vol. 5, p. 29, 2018.

[25] L. Heilbronn, A. Srikrishna, and D. Peffley, "Neutron fluences in lunar habitats," in *2015 IEEE Aerospace Conference*, 2015, pp. 1–6.

[26] F. Ruess, J. Schaenzlin, and H. Benaroya, "Structural design of a lunar habitat," *Journal of Aerospace Engineering*, vol. 19, no. 3, pp. 133–157, 2006.

[27] S. Jason, A. da Silva Curiel, L. Gomes, A. Phipps, J. Ward, W. Sun, and M. Sweeting, "Low cost planetary exploration: surrey lunar minisatellite and interplanetary platform missions," *Acta Astronautica*, vol. 48, no. 5, pp. 669–680, 2001.

[28] R. Biesbroek and G. Janin, "Ways to the Moon," *ESA bulletin*, vol. 103, pp. 92–99, 2000.

[29] C. Uphoff, "Practical aspects of transfer from GTO to lunar orbit," NASA, Ball Space Systems Division, Technical Report 93N24719, 1993.

[30] R. Sandau, H.-P. Roeser, A. Valenzuela, and Others, *Small satellite missions for earth observation*. Springer, 2014.

[31] R. M. Myers, S. R. Oleson, F. M. Curran, and S. J. Schneider, "Small satellite propulsion options," NASA, Lewis Research Cebter, Technical Memorandum 106701, 1994.

[32] NFPA, *Fire protection guide to hazardous materials*, 14th ed. National Fire Protection Association, 2010.

[33] J. Kreider, *Medium and High Temperature Solar Processes*. New York: Energy Science and Engineering; Academic Press, Inc., 1979.

[34] P. Henshall, "A Proposal to Develop and Test a Fibre-Optic Coupled Solar Thermal Propulsion System for Microsatellites," Surrey University Guildford, United Kingdom, Tech. Rep. 0704-0188, 2006.

[35] J. E. Midwinter, *Optical fibers for transmission*. New York: Wiley, 1979.

[36] D. Rodriguez-Sanchez and G. Rosengarten, "Improving the concentration ratio of parabolic troughs using a second-stage flat mirror," *Applied Energy*, vol. 159, pp. 620–632, dec 2015.

[37] T. Nakamura, B. K. Smith, and R. J. Gustafson, "Solar Thermal Power System for Oxygen Production from Lunar Regolith: Engineering System Development," in *Joint Annual Meeting of LEAG,ICEUM, and SRR*, vol. 1446, 2008, p. 95.

[38] R. K. Shaltens and L. S. Mason, "Early results from solar dynamic space power system testing," *Journal of Propulsion and Power*, vol. 12, no. 5, pp. 852–858, sep 1996.

[39] P. Frye and C. Kudija, "Integrated solar upper stage engine ground demonstration test results and data analysis," in *34th AIAA/ASME/SAE/ASEE Joint Propulsion Conference and Exhibit*, 1998, p. 3958.

[40] H. Sahara and M. Shimizu, "Solar Thermal Propulsion System for Microsatellites Orbit Transferring," in *40th AIAA/ASME/SAE/ASEE Joint Propulsion Conference and Exhibit*, jul 2004.

[41] J. Pearson Jr, P. Gierow, and D. Lester, "Near term in-space demonstration of an inflatable concentrator," in *37th Aerospace Sciences Meeting and Exhibit*, 1999, p. 1073.

[42] T. Nakamura, D. Sullivan, J. McClanahan, J. Shoji, R. Partch, and S. Quinn, "Solar Thermal Propulsion for Small Spacecraft," in *40th AIAA/ASME/SAE/ASEE Joint Propulsion Conference and Exhibit*, no. July, 2004, pp. 1–11.

[43] T. L. Bergman, F. P. Incropera, D. P. DeWitt, and A. S. Lavine, *Fundamentals of heat and mass transfer*, 7th ed. John Wiley & Sons, 2011.

[44] D. L. Trimm, S. Akashah, A. Bishara, and M. Absi-Halabi, *Catalysts in Petroleum Refining 1989*, ser. Studies in Surface Science and Catalysis. Elsevier Science, 1990, vol. 53.

[45] P. Colonna, N. R. Nannan, A. Guardone, and E. W. Lemmon, "Multiparameter equations of state for selected siloxanes," *Fluid Phase Equilibria*, vol. 244, no. 2, pp. 193–211, 2006.

[46] M. Preißinger and D. Brüggemann, "Thermal stability of hexamethyldisiloxane (MM) for high-temperature organic Rankine cycle (ORC)," *Energies*, vol. 9, no. 3, p. 183, 2016.

[47] S. Bahamonde, M. Pini, C. De Servi, A. Rubino, and P. Colonna, "Method for the Preliminary Fluid Dynamic Design of High-Temperature Mini-Organic Rankine Cycle Turbines," *Journal of Engineering for Gas Turbines and Power*, vol. 139, no. 8, p. 82606, 2017.

[48] P. Colonna and T. P. der Stelt, "FluidProp: a program for the estimation of thermo physical properties of fluids," http://www. FluidProp. com, 2004.

[49] M. Moran, H. Shapiro, D. Boettner, and M. Bailey, *Fundamentals of engineering thermodynamics*. John Wiley & Sons, 2010.

[50] P. Reynolds, William; and Colonna, "Vapor power plants," in *Thermodynamics*. Cambridge University Press, 2018, ch. 7.

[51] S. Kim, J. Kim, and I. Mudawar, "Flow condensation in parallel micro-channels–Part 1: Experimental results and assessment of pressure drop correlations," *International journal of heat and mass transfer*, vol. 55, no. 4, pp. 971–983, 2012.

[52] S. Kim and I. Mudawar, "Universal approach to predicting two-phase frictional pressure drop for adiabatic and condensing mini/micro-channel flows," *International Journal of Heat and Mass Transfer*, vol. 55, no. 11-12, pp. 3246–3261, 2012.

[53] S. Kim and I. Mudawar, "Universal approach to predict-

ing heat transfer coefficient for condensing mini/micro-channel flow," *International Journal of Heat and Mass Transfer*, vol. 56, no. 1-2, pp. 238–250, 2013.

[54] S. Kim and I. Mudawar, "Flow condensation in parallel micro-channels. Part 2: Heat transfer results and correlation technique," *International Journal of Heat and Mass Transfer*, vol. 55, no. 4, pp. 984–994, 2012.

[55] D. Gilmore, *Spacecraft thermal control handbook, Volume I: fundamental technologies*. American Institute of Aeronautics and Astronautics, Inc., 2002.

[56] G. P. Sutton and O. Biblarz, *Rocket propulsion elements*. John Wiley & Sons, 2016.

[57] G. Welsch, R. Boyer, and E. W. Collings, *Materials properties handbook: titanium alloys*. ASM international, 1993.

[58] D. H. Huang and D. K. Huzel, *Modern engineering for design of liquid-propellant rocket engines*. American Institute of Aeronautics and Astronautics, 1992.

[59] E. Sato, S. Sawai, K. Uesugi, T. Takami, K. Furukawa, M. Kamada, and M. Kondo, "Superplastic titanium tanks for propulsion system of satellites," in *Materials science forum*, vol. 551. Trans Tech Publ, 2007, pp. 43–48.

[60] J. R. Wertz and W. J. Larson, *Space mission analysis and design*, 3rd ed. Torrance, California: Microcosm Press, 1999.

[61] D. Simon, "Biogeography-Based Optimization," *IEEE Transactions on Evolutionary Computation*, vol. 12, no. 6, pp. 702–713, dec 2008.

[62] D. Liang, L. Fraser Monteiro, M. Ribau Teixeira, M. Fraser Monteiro, and M. Collares-Pereira, "Fiber-optic solar energy transmission and concentration," *Solar Energy Materials and Solar Cells*, vol. 54, no. 1-4, pp. 323–331, jul 1998.

[63] A. C. Caputo, P. M. Pelagagge, and P. Salini, "Joint economic optimization of heat exchanger design and maintenance policy," *Applied Thermal Engineering*, vol. 31, no. 8-9, pp. 1381–1392, jun 2011.

[64] J. Wang, Z. Yan, M. Wang, M. Li, and Y. Dai, "Multi-objective optimization of an organic Rankine cycle (ORC) for low grade waste heat recovery using evolutionary algorithm," *Energy Conversion and Management*, vol. 71, pp. 146–158, 2013.

[65] F. Kennedy, "Solar Thermal Propulsion for Microsatellite Manoeuvring," PhD Thesis, University of Surrey, 2004.

[66] P. Olla, *Space technologies for the benefit of human society and earth*. Dordrecht: Springer, 2009.

[67] E. Lemmon, M. Huber, and M. McLinden, "NIST REFPROP v9. 1 Reference fluid thermodynamic and transport properties," 2013.

[68] MatWeb, "MatWeb, The Online Materials Information Resource," http://www/matweb.com/, 2002.

[69] H. Soliman, "The mist-annular transition during condensation and its influence on the heat transfer mechanism," *International Journal of Multiphase Flow*, vol. 12, no. 2, pp. 277–288, 1986.

[70] S. M. Zivi, "Estimation of steady-state steam void-fraction by means of the principle of minimum entropy production," *Journal of heat transfer*, vol. 86, no. 2, pp. 247–251, 1964.

BIOGRAPHY

Fiona Leverone *received her B.Sc and M.Sc in Mechanical Engineering in 2011 and 2014 respectively from the University of KwaZulu-Natal in South Africa, where she also lectured in Engineering Design. Her MSc research was on hybrid rocket propulsion for sub-orbital rockets. Fiona is now a Ph.D candidate at the Delft University of Technology in the Netherlands and is focusing on investigating the feasibility of an integrated solar thermal system that is capable of co-generating electrical power and propulsion for small satellite applications.*

Angelo Cervone *is an Assistant Professor in the Aerospace Engineering Faculty at Delft University of Technology. He holds a PhD in aerospace propulsion from University of Pisa (Italy), followed by a 2-years post-doc fellowship at Osaka University (Japan). His main research areas are micro-propulsion, small satellites, systems engineering, cavitation and flow instabilities in liquid rocket engine turbopumps, innovative interplanetary small satellite missions. He is author or co-author of more than 120 papers published in peer-reviewed journals or presented at international conferences. He is member of the Space Propulsion Technical Committee of the International Astronautical Federation, and serves as chairman for several international conferences related to space propulsion.*

Matteo Pini *graduated in energy engineering from Politecnico di Milano and obtained the PhD from the same University specializing on design methods for novel and unconventional turbomachinery. He is currently Assistant Professor within the Propulsion and Power group of the faculty of Aerospace Engineering at the Delft University of Technology where he is leading the research on turbomachinery for aerospace systems.*

Eberhard Gill *received a diploma in physics and holds a PhD in theoretical astrophysics of the Eberhard-Karls-University Tuebingen, Germany. He holds a Master of Space Systems Engineering of the Delft University of Technology. Since 2007, he holds the Chair of Space Systems Engineering at the Faculty of Aerospace Engineering of the Delft University of Technology. He is also the Director of TU Delft Space Institute. The research interests of Dr. Gill are miniaturized space systems, navigation, distributed space systems and Systems Engineering. Dr. Gill has authored or co-authored more than 250 journal articles and conference papers and four text books: Relativity and the Earth's Rotation (Springer 1990), Satellite Orbits (Springer 2000), Applied Space Systems Engineering (McGraw-Hill 2009) and Distributed Space Missions for Earth System Monitoring (Springer 2013).*